고이득 관측기를 이용한 자기 베어링 휠용 자기 부상 시스템의 비선형 제어

Nonlinear Control of an Electromagnetic Levitation System Using High-gain Observers for Mmagnetic Bearing Wheels

최 호 림*, 신 희 섭, 구 민 성, 임 종 태, 김 용 민
(Ho-Lim Choi, Hee-Sub Shin, Min-Sung Koo, Jong-Tae Lim, and Yong-Min Kim)

Abstract: In this paper, we develop a functional test model for magnetic bearing wheels. The functional test model is an electromagnetic levitation system that has three degree of freedom, which consists of one axial suspension from gravity and two axes gimbaling capability to small angels. A nonlinear controller with high-gain observers is proposed and the real-time experiment results show that the rotor is accurately levitated at the desired position and well-balanced, which is a suitable result for the potential use an magnetic bearing wheels. Also, the proposed scheme exhibits better performance when it is compared with the conventional PID control method.

Keywords: electromagnetic levitation, nonlinear systems, feedback linearization, high-gain observers, magnetic bearing wheel

I. INTRODUCTION

In general, a spacecraft in orbit is equipped with reaction wheels serving as actuators in the attitude control system and ball bearing wheels have been dominantly used in reaction wheels. However, among various kinds of on-board system components, ball bearing wheels have been identified as one of the main sources of vibration noise due to the wear in mechanical contact of a rotor, residual imbalances, and bearing imperfections [1]. These problems can be greatly reduced by using magnetic bearing wheels. Magnetic bearing wheels can suspend the rotor by the magnetic or electromagnetic forces with high-precision and high-rotational speed of the rotor, no mechanical contact, and no use of lubrication [2].

For the development of magnetic bearing wheels, there have been several results reported in [2-4]. The main component of magnetic bearing wheels is the electromagnetic levitation system (EMLS) which is usually modeled as a nonlinear system [5-10]. Interestingly, the EMLS is often feedback linearizable such that various feedback linearizing control approach yields a better performance over the conventional linear approach [4,6]. The nonlinear controllers in [4] and [6] use full state information while our method is an output feedback control scheme. Moreover, in our approach, we can use ε to reduce the disturbance effect.

In this paper, we use a functional test model (FTM), which is an EMLS, for magnetic bearing wheels. In the FTM, the active control of three degrees of freedom is possible, which consists of one axial suspension from gravity and two axes gimbaling capability to small angles. A feedback linearizing nonlinear controller with a gain-scaling factor is proposed and high-gain observer is used in order to estimate the velocities of levitation and gimbal angles of the rotor. The theoretical backgrounds of the proposed control technique and high-gain observer are well addressed in [11,12] and [13,14], respectively. In particular, the high-gain observer is robust against model uncertainty and its structure is continuous unlike the sliding-mode observer used in [15]. This new 'feedback linearizing nonlinear controller with a gain-scaling factor' has advantage over the traditional feedback linearizing controller used in [4,6,9] in the sense that its robustness against system uncertainty and systematic design procedures are well addressed.

Experiment results show that the proposed controller achieves the accurate positioning of the rotor under the narrow gap condition, which is a suitable result for magnetic bearing wheels. The proposed nonlinear control approach exhibits improved performance over the previously designed conventional PID control approach in [1], which is consistent with results reported in [4,6]. Moreover, the stability analysis with a simple systematic controller design procedure is given, which can be a guideline in tuning controller gains for control engineers.

II. MODEL OF THE ELECTROMAGNETIC LEVITATION SYSTEM

Fig. 1 shows the schematic diagram of the FTM that has three degrees of freedom which consists of z axis suspension from gravity, and x and y axes gimbaling capability to small angles. The meanings of symbols used in Fig. 1 are summarized in Table 1. The FTM is built in a way that four electromagnets levitate the rotor when the currents are engaged into each electromagnet. The dynamics of the FTM is

$$m\ddot{z} = f_1 + f_2 + f_3 + f_4 - mg,\ I\ddot{\phi} = T_x,\ I\ddot{\theta} = T_y \qquad (1)$$

where m is the mass of the rotor, I is the moment of inertia of the rotor for the x and y axes, g is the gravitational force, and T_x and T_y are the torques of the x and y axes. Each torque can be represented by

$$T_x = W_e(f_2 - f_4),\ T_y = W_e(f_3 - f_1) \qquad (2)$$

* 책임저자(Corresponding Author)
논문접수: 2009. 1. 15., 채택확정: 2009. 3. 11.
최호림: 동아대학교 전기공학과(hlchoi@dau.ac.kr)
신희섭, 구민성, 임종태: 한국과학기술원 전기 및 전자공학과
(ahwahs@kaist.ac.kr/goose@kaist.ac.kr/jtlim@stcon.kaist.ac.kr)
김용민: 한국과학기술원 인공위성연구센터(ymkim@rtcl.kaist.ac.kr)
※ 이 논문은 동아대학교 학술연구비 지원에 의하여 연구되었음.

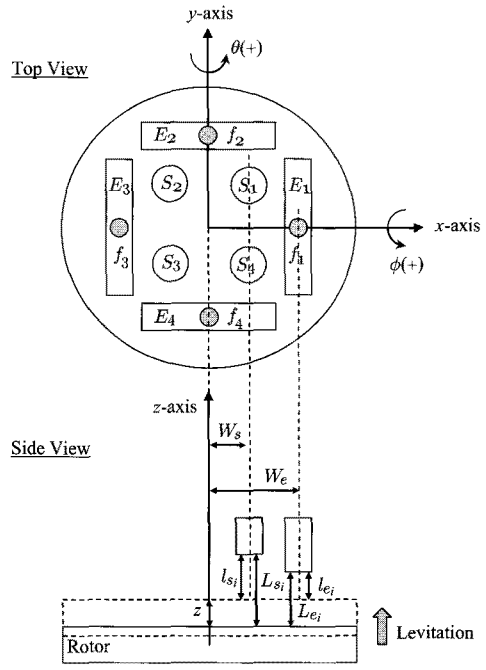

그림 1. FTM의 개요도.

Fig. 1. Schematic diagram of the FTM.

Under the assumption that the angle displacement of the rotor are small, the approximate equations of gap sensor measurement l_{s_i} can be expressed as follows [1].

$$\begin{aligned} l_{s_1} &= L_{s_1} - z + W_s\theta - W_s\phi \\ l_{s_2} &= L_{s_2} - z - W_s\theta - W_s\phi \\ l_{s_3} &= L_{s_3} - z - W_s\theta + W_s\phi \\ l_{s_4} &= L_{s_4} - z + W_s\theta + W_s\phi \end{aligned} \tag{3}$$

Then, from (3) and the structure of the FTM, z, ϕ, and θ can be obtained using the gap sensor measurement l_{s_i} as follows [1].

표 1. FTM의 개요도에 쓰인 심볼의 의미.

Table 1. Meanings of symbols in schematic diagram of the FTM.

Symbol	Meaning (for $i = 1, \cdots, 4$ where applicable)
E_i	Electromagnet
f_i	Electromagnetic forces generated by electromagnet
S_i	Gap sensor
ϕ	Rotational angle of the x axis
θ	Rotational angle of the y axis
z	z axis displacement
W_s	Length from the center of the rotor to the gap sensor
W_e	Length from the center of the rotor to the electromagnet
l_{s_i}	Gap sensor measurement: displacement from the gap sensor to the rotor
l_{e_i}	Displacement from the electromagnet to the rotor
L_{s_i}	Distance from the gap sensors to the rotor at the ground position
L_{e_i}	Displacement from the electromagnet to the rotor at the ground position

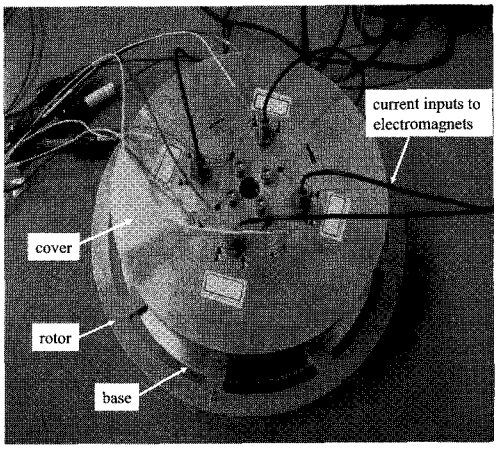

그림 2. FTM의 원형.

Fig. 2. Prototype of the FTM.

$$\begin{aligned} z &= \frac{1}{4}[(L_{s_1} + L_{s_2} + L_{s_3} + L_{s_4}) - (l_{s_1} + l_{s_2} + l_{s_3} + l_{s_4})] \\ \phi &= \frac{1}{4W_s}[(l_{s_3} + l_{s_4} - l_{s_1} - l_{s_2}) - (L_{s_3} + L_{s_4} - L_{s_1} - L_{s_2})] \\ \theta &= \frac{1}{4W_s}[(l_{s_1} + l_{s_4} - l_{s_2} - l_{s_3}) - (L_{s_1} + L_{s_4} - L_{s_2} - L_{s_3})] \end{aligned} \tag{4}$$

Finally the actual FTM is shown in Fig. 2. The four electromagnets and sensors are attached inside the cover of the system, and the rotor stays on the base. Thus, the cover is equivalent to the stator and the base supports the rotor. Four pairs of electromagnets with coils are used to generate the electromagnetic forces to pull the rotor in the z direction for levitation. Four gap sensors are used to measure the suspension displacement of the rotor.

III. CONTROLLER DESIGN USING HIGH-GAIN OBSEREVRS

1. Quarter-model approach

Our control objective is to levitate the rotor to a certain height while keeping the gimbal angles to zeros such that the rotor is well-balanced while it is levitated on the flat platform. Thus, the system can be a high-performance magnetic bearing used for reaction wheels in a satellite. The FTM has four electromagnets and our first control approach is to divide the system into four pieces as shown in Fig. 3 where x_i denotes the actual height of each piece.

The relation between each coil current and electromagnetic

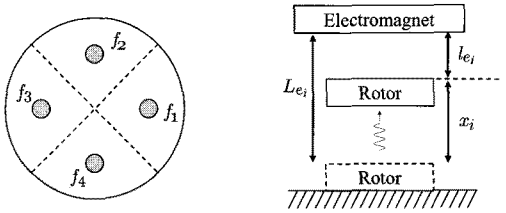

(a) Four divided system (b) Description of each quarter model

그림 3. 4분기 모델.

Fig. 3. Quarter-model.

force is described by

$$i_i = \frac{l_{e_i}}{n}\sqrt{\frac{8f_i}{\mu_0 G}}, \quad i = 1,\cdots,4 \tag{5}$$

where i_i is the coil current of the ith electromagnet, n is the number of coil turn, μ_0 is the magnetic permeability in the air, and G is the cross are of each electromagnet.

Then, when we consider only the quarter-model of the system, we obtain the following system dynamics similarly to (1) by taking one quarter of rotor mass and assuming only single electromagnetic force f_i is applied to each piece. For $i = 1,\cdots,4$, we have

$$\frac{m}{4}\ddot{x}_i = f_i - \frac{mg}{4} \tag{6}$$

Then, we obtain the following SISO nonlinear system from (5) and (6).

$$\ddot{x}_i = \frac{\mu_0 G}{2m}\frac{n^2 u_i}{(L_{e_i} - x_i)^2} - g \tag{7}$$

where we let $u_i = i_i^2$ as a control input.

Letting $x_i = x_{i_1}$ and $\dot{x}_i = x_{i_2}$ and considering the possible model uncertainty caused from any deviation between ideal and actual model, we obtain the following feedback linearizable second-order nonlinear system. For $i = 1,\cdots,4$, the four quarter-model systems are

$$\begin{aligned}\dot{x}_{i_1} &= x_{i_2} + \delta_{i_1}(t, x_i, u_i)\\ \dot{x}_{i_2} &= \frac{\mu_0 G}{2m}\frac{n^2 u_i}{(L_{e_i} - x_{i_1})^2} - g + \delta_{i_2}(t, x_i, u_i)\end{aligned} \tag{8}$$

where $\delta_{i_j}(t, x_i, u_i)$, $j = 1,2$ denote model uncertainty with an assumption that $\delta_{i_j}(t, x_i, u_i) \le c(|x_{i_1}| + |x_{i_j}|)$, $j = 1,2$.

Now, our control approach is to design a robust nonlinear controller which sends each x_{i_1} to a reference height z_{ref}. That is, when each designed controller levitates its own piece of rotor, the rotor will be levitated robustly at the desired position overall. Under the designed FTM environment, x_{i_1} is the only available information from the sensor measurement. Thus, we design the following high-gain observer to estimate the velocity of x_{i_1}. The high-gain observer is designed by copying the system equation plus an error injection term with a high-gain factor ε_L. The robustness of high-gain observer with ε_L is well-addressed in the literature [12-14].

$$\begin{aligned}\dot{\hat{x}}_{i_1} &= \hat{x}_{i_2} - \frac{l_1}{\varepsilon_L}(x_{i_1} - \hat{x}_{i_1})\\ \dot{\hat{x}}_{i_2} &= \frac{\mu_0 G}{2m}\frac{n^2 u_i}{(L_{e_i} - x_{i_1})^2} - g - \frac{l_2}{\varepsilon_L^2}(x_{i_1} - \hat{x}_{i_1})\end{aligned} \tag{9}$$

where $\varepsilon_L > 0$ is a high-gain factor to be adjusted.

The observer gains l_1 and l_2 are selected such that the following matrix A_L becomes Hurwtiz.

$$A_L = \begin{bmatrix} l_1 & 1 \\ l_2 & 0 \end{bmatrix} \tag{10}$$

Now, with the observer, the following feedback linearizing controller is introduced. The first multiplicative term is to cancel the input nonlinearity.

$$u_i = \frac{2m}{\mu_0 G}\frac{(L_{e_i} - x_{i_1})^2}{n^2}\left(\frac{k_1}{\varepsilon_K^2}(x_{i_1} - z_{ref}) + \frac{k_2}{\varepsilon_K}\hat{x}_{i_2} + g\right) \tag{11}$$

For the selection of controller parameters, k_1 and k_2 are selected such that the following matrix A_K becomes Hurwtiz.

$$A_K = \begin{bmatrix} k_1 & 1 \\ k_2 & 0 \end{bmatrix} \tag{12}$$

The gain-scaling factor $\varepsilon_K > 0$ has a function of adjusting the controller speed and robustness. As ε_K becomes smaller, the controller has more robustness against the triangular-type model uncertainty and achieves a faster system response due to the high-gain control input. The theoretical results in [11,12] regarding the robustness of proposed control and observer along with selection of A_K, A_L, ε_K, ε_L is briefly addressed in the Appendix.

2. Compensation for two rotational angles

In the previous section, the nonlinear controllers are designed for each quarter-model system independently. However, as shown in Fig. 1, there are two gimbal angles ϕ and θ along the x and y axes. Since our control goal is to keep the rotor well-balanced, it is important to keep ϕ and θ at zero. As noted in (1) and (2), θ is related with two forces f_1 and f_3 and ϕ is related with two forces f_2 and f_4. Thus, it is reasonable to assume that θ and ϕ are decoupled from each other. Due to the fact that the lifting speed of each quarter model is somewhat different because of model uncertainty, there may be imbalance of rotor during the transient period. Thus, we need to add a compensator to the controller developed in (11) for compensating the gimbal angle θ. From (1), (2) and (5), we have the following dynamics.

$$\ddot{\theta} = \frac{W_e \mu_0 G n^2}{8I}\left(\frac{u_3}{(L_{e_3} - x_{3_1})^2} - \frac{u_1}{(L_{e_1} - x_{1_1})^2}\right) \tag{13}$$

Letting $\theta = \eta_1$ and $\dot{\theta} = \eta_2$, we obtain

$$\begin{aligned}\dot{\eta}_1 &= \eta_2\\ \dot{\eta}_2 &= \frac{W_e \mu_0 G n^2}{8I}\left(\frac{u_3}{(L_{e_3} - x_{3_1})^2} - \frac{u_1}{(L_{e_1} - x_{1_1})^2}\right)\end{aligned} \tag{14}$$

Since only η_1 is available as noted in (4), we again design the following high-gain observer to estimate the velocity of η_1.

$$\begin{aligned}\dot{\hat{\eta}}_1 &= \hat{\eta}_2 - \frac{l_1}{\varepsilon_L}(\eta_1 - \hat{\eta}_1)\\ \dot{\hat{\eta}}_2 &= \frac{W_e \mu_0 G n^2}{8I}\left(\frac{u_3}{(L_{e_3} - x_{3_1})^2} - \frac{u_1}{(L_{e_1} - x_{1_1})^2}\right) - \frac{l_2}{\varepsilon_L^2}(\eta_1 - \hat{\eta})\end{aligned} \tag{15}$$

where the selection rules of l_2, and ε_L are the same as in (9).

Now, with the estimated $\hat{\eta}_2$, the controller in (11) is modified into the final form as follows by adding the balancing compensation term. For controllers u_1 and u_3, we have

$$u_1 = \frac{2m}{\mu_0 G}\frac{(L_{e_1}-x_{1_1})^2}{n^2}\left(\frac{k_1}{\varepsilon_K^2}(x_{1_1}-z_{ref})+\frac{k_2}{\varepsilon_K}\hat{x}_{1_2}+\Delta_1\right)$$
$$u_3 = \frac{2m}{\mu_0 G}\frac{(L_{e_3}-x_{3_1})^2}{n^2}\left(\frac{k_1}{\varepsilon_K^2}(x_{3_1}-z_{ref})+\frac{k_2}{\varepsilon_K}\hat{x}_{3_2}+\Delta_3\right) \quad (16)$$

where $\Delta_1 = g + a_1\eta_1 + a_2\hat{\eta}_2$, $\Delta_3 = g + b_1\eta_1 + b_2\hat{\eta}_2$, the compensator gains a_1, a_2, b_1, and b_2 are to be selected.

Now, for two quarter-models ($i = 1$ and 3) in (8) and gimbal angle θ dynamics in (14), the closed-loop system with the controller (16) and observers (9) and (15) is summarized as follows.

$$\dot{\Xi} = \begin{bmatrix} A & * & * & * \\ 0 & A_L(\varepsilon_L) & 0 & 0 \\ 0 & 0 & A_L(\varepsilon_L) & 0 \\ 0 & 0 & 0 & A_L(\varepsilon_L) \end{bmatrix}\Xi \quad (17)$$

where

$\Xi = [X, \tilde{X}_1, \tilde{X}_3, \tilde{\eta}]^T$,

$X = [x_{1_1} - z_{ref}, x_1, x_{3_1} - z_{ref}, x_{3_2}, \eta_1, \eta_2]\hat{}T$,

$\tilde{X}_1 = [x_{1_1} - \hat{x}_{1_1}, x_{1_2} - \hat{x}_{1_2}]^T$, $\tilde{X}_3 = [x_{3_1} - \hat{x}_{3_1}, x_{3_2} - \hat{x}_{3_2}]^T$,

$\tilde{\eta} = [\eta_1 - \hat{\eta}_1, \eta_2 - \hat{\eta}_2]^T$, and

$$A = \begin{bmatrix} 0 & 1 & 0 & 0 & 0 & 0 \\ \frac{k_1}{\varepsilon_K^2} & \frac{k_2}{\varepsilon_K} & 0 & 0 & a_1 & a_2 \\ 0 & 0 & 0 & 1 & 0 & 0 \\ 0 & 0 & \frac{k_1}{\varepsilon_K^2} & \frac{k_2}{\varepsilon_K} & b_1 & b \\ 0 & 0 & 0 & 0 & 0 & 1 \\ -a\frac{k_1}{\varepsilon_K^2} & -a\frac{k_2}{\varepsilon_K} & a\frac{k_1}{\varepsilon_K^2} & a\frac{k_2}{\varepsilon_K} & \Gamma & \Pi \end{bmatrix} \quad (18)$$

where $\Gamma = a(b_1 - a_1)$, $\Pi = a(b_2 - a_2)$ with $a = \frac{W_e m}{4I}$ and

$$A_L(\varepsilon_L) = \begin{bmatrix} \frac{l_1}{\varepsilon_L} & 1 \\ \frac{l_2}{\varepsilon_L^2} & 0 \end{bmatrix} \quad (19)$$

The design procedure of the controller parameters are summarized as follows.

(i) Select the pairs of gains (k_1, k_2) and (l_1, l_2) such that A_K and A_L are Hurwitz,

(ii) Select high-gain factors $\varepsilon_K > 0$ and $\varepsilon_L > 0$ in order to adjust the controller and estimator convergence speed and their robustness. In practice, we choose $\varepsilon_K, \varepsilon_L << 1$ to provide fast system response, fast observer convergence, and robustness against uncertainty.

(iii) Select the compensator gains a_1, a_2, b_1, and b_2 to make the matrix A Hurwitz.

Noting that $A_L(\varepsilon_L)$ is Hurwitz for all $\varepsilon_L > 0$ when A_L is Hurwitz. It is easy to check that the closed-loop system (17) becomes stable by following the above design procedure. Finally, the other quarter-model systems (8) for $i = 2$ and 4 and the gimbal angle ϕ dynamics have the same structure. Thus, the nonlinear controllers u_2 and u_4 can be analogously designed for the other electromagnets E_2 and E_4 and the detals are omitted.

Remark 1: Note that the closed-loop model (18) has some algebraic constraints in the sense that the states in X are not independent. That is, η_1 and η_2 depend on x_{1_1}, x_{1_2}, x_{2_1}, and x_{2_2}. However, the overall stability is still valid because the convergence of Ξ to zero leads the convergence of each state to zero as well.

IV. EXPERIMENT STUDY

1. Experiment setup

The major mechanical specification of the FTM is described in Table 2. Fig. 4 shows the block diagram of system electronics to control the FTM and Fig. 5 shows the actual hardware setup. The main processor unit mainly consists of a 32-bit floating-point digital signal processor (DSP) TMS320C32 from Texas Instruments, a 12-bit analog-to-digital converter (ADC), and a digital-to-analog converter (DAC). This DSP is adequate for fast computation. It operates 30 million instructions per second (MIPS) in 60MHz clock speed and is equipped with two 256×32 on-chip RAM blocks, one serial port, two 32-bit timer interrupts, and two DMA interrupts. The 12-bit ADC and the DAC are used to read the output from the gap sensor and to generate the control inputs to electromagnets, respectively. The ADC has 4 channels and conversion time is 3μs and the range of the input voltage is from -5V to 5V. The conversion time of DAC is 10μs and the range of the output voltage is from 0V to 10V.

The power module is used for the current control of the FTM, which converts the output voltage of DAC to a suitable current and transmits the current into the coil of the electromagnet. The power module is linear-typed and the maximum output current is

표 2. FTM의 물리적 파라미터.

Table 2. Physical parameters of the FTM.

Physical quantities	Values
W_s	0.018725(m)
W_e	0.026(m)
L_{s_i}	0.0013(m)
L_{e_i}	0.0008(m)
m	0.722(kg)
n	240
I	0.000877362(kg - m^2)
μ_0	$4\pi \times 10^{-7}$(N/A^2)
G	0.000100530944(m^2)
g	9.81(m/s^2)

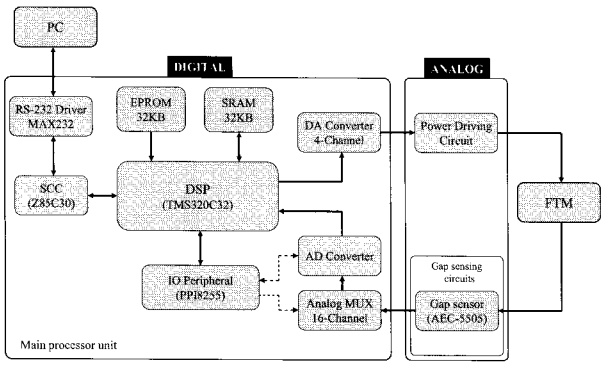

그림 4. 전자 제어 장치의 다이어그램.
Fig. 4. Block diagram of control electronics.

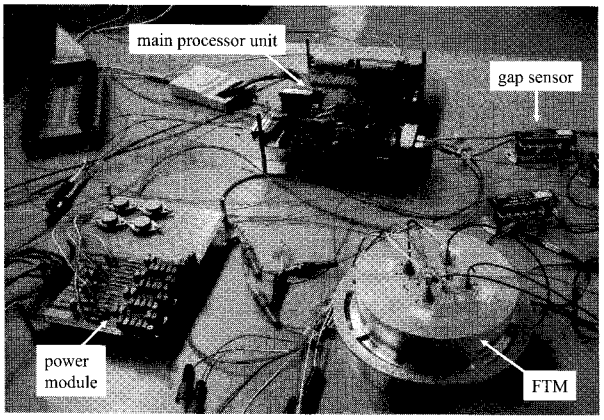

그림 5. 실험장치.
Fig. 5. Experiment setup.

1A and it can be adjusted with the variable register attached in the differential amplifier. The AEC-5505 model of eddy current-typed gap sensors from Applied Electronics Co., Ltd is used to measure each distance. The resolution of gap sensor is 5μm.

The electromagnets mounted in the FTM are SUS410 ferromagnetic material made by stainless steel. In our test, we observe that the electromagnetic field is formed closely around each electromagnet. Therefore, the interference of the electromagnetic field between the neighboring electromagnets is very small, which is a desirable phenomenon for the control of the electromagnetic force of each electromagnet. The control algorithm is written in Visual C++ with a sampling rate of 1kHz on a standard IBM PC and then it is loaded into the DSP system operation. Data acquisition program is also written in order to store all necessary experiment results. For communication with PC, a serial communication controller (SCC) Z85C30 and IO ports 82C55A are used..

1.1 Experiment results

We set a reference as $[z_{ref}, \phi_{ref}, \theta_{ref}] = [0.3\text{mm}, 0\text{deg}, 0\text{deg}]$ such that rotor can be freely rotated while levitated at $z = 0.3$mm without touching the cover or base of the FTM. Since L_{e_i} is only 0.8mm, it is important to reduce any overshoot in the control response to avoid any physical contact. According to the design procedure given previously, we choose $k_1 = -2.25$, $k_2 = -3$ and $l_1 = l_2 = -4$ to make A_K and A_L Hurwitz, respectively. The eigenvalues of A_K and A_L are placed at -1.5 and -2, respectively so that the damping ratio is 1 and it is expected that there is no overshoot in the system response. Then, for the gain-scaling and high gain factors, we choose $\varepsilon_K = 0.0082$ and $\varepsilon_L = 0.02$. Note that some extremely small values of $\varepsilon_K, \varepsilon_L$ (less than 0.001) may cause input saturation and system failure. For the gimbal angles compensator gains, $a_1 = a_2 = 200$ and $b_1 = b_2 = -400$ are selected.

In the previous control approach in [1], a conventional PID controller is designed due to its simplicity. The PID controller used in [1] takes the form of

$$u = K_P e + K_D \frac{de}{dt} + K_I \int_0^t e(\tau) d\tau \tag{20}$$

where $u = [f_z, T_x, T_y]^T$, $e = [z - z_{ref}, \phi - \phi_{ref}, \theta - \theta_{ref}]^T$, and the force f_z and the torques T_x, T_y are distributed to each electromagnet of the FTM using the least squares method as follows [1].

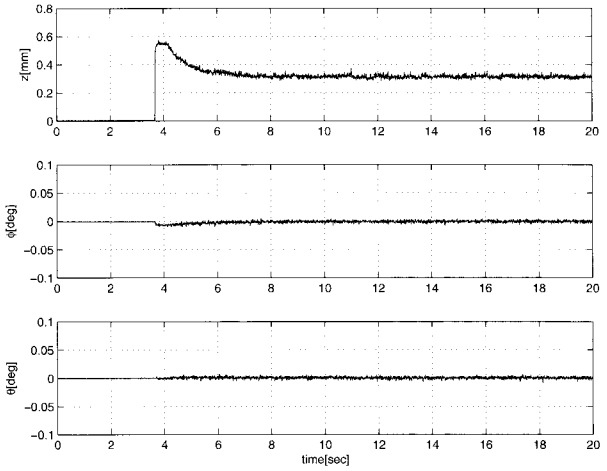

(a) Rotor levitation and gimbal angles

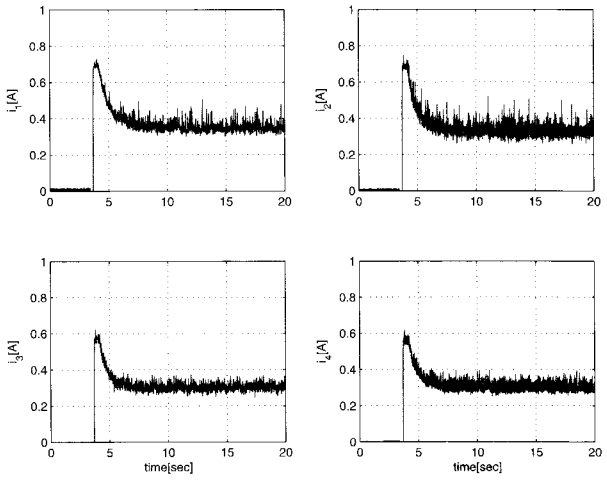

(b) Current inputs

그림 6. 기존의 PID 제어기에 의한 실험 결과.
Fig. 6. Experiment result by the conventional PID controller.

$$
\begin{aligned}
f_1 &= \frac{1}{4}(f_z + mg) - \frac{1}{2}\frac{T_y}{W_e} \\
f_2 &= \frac{1}{4}(f_z + mg) + \frac{1}{2}\frac{T_x}{W_e} \\
f_3 &= \frac{1}{4}(f_z + mg) + \frac{1}{2}\frac{T_y}{W_e} \\
f_4 &= \frac{1}{4}(f_z + mg) - \frac{1}{2}\frac{T_x}{W_e}
\end{aligned} \tag{21}
$$

In [1], the selected PID gains are $K_p = \text{diag}[1000,20,20]$, $K_I = \text{diag}[5000,8.33,8.33]$, and $K_D = \text{diag}[100,0.013,0.013]$. When we compare the performances of both control approaches in the actual experiment, the conventional PID controller exhibits a slower response with some large overshoot. This overshoot leads to more consumption of current, which is not adequate for the embedded system with limited resource like a satellite. As shown in Figs. 6-7, we observe that the proposed nonlinear controller shows more uniform control inputs and smaller deviations in gimbal angles ϕ and θ at the steady state. The performance differences can be clearly seen through the tracking error comparison in Fig. 8. The experiment results are consistent with simulation results with an acceptable error. In order to check the controller response against the external disturbance, we slightly raise the rotor using a small stick for a few seconds and then remove stick. As shown in Fig. 9, the rotor is quickly returned to the reference position without any notable overshoot. From this experiment, we observe that the proposed nonlinear control approach is more adequate since the FTM will be eventually targeted for reaction wheel as an attitude control system in a satellite. Moreover, it is shown that the proposed control can be designed more systematically along with stability analysis whereas the conventional PID controller is more an ad-hoc based linear approach.

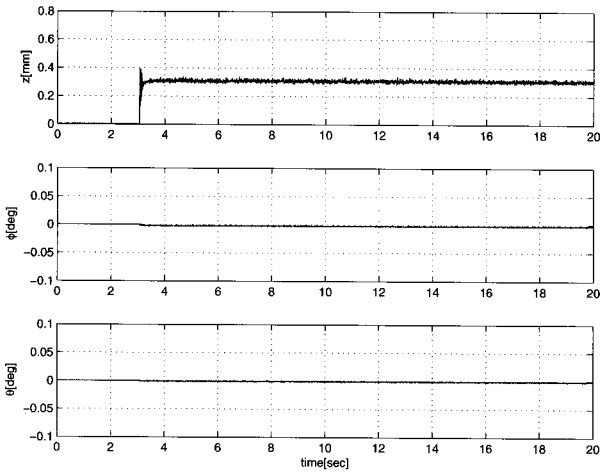

(a) Rotor levitation and gimbal angles

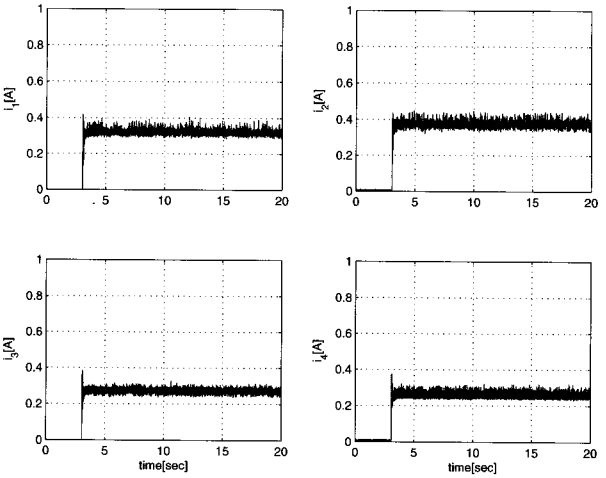

(b) Current inputs

그림 7. 제안된 제어기에 의한 실험 결과.

Fig. 7. Experiment result by the proposed controller.

V. CONCLUSIONS

In this paper, we have developed an electromagnetic levitation system for magnetic bearing wheels. A nonlinear controller with a

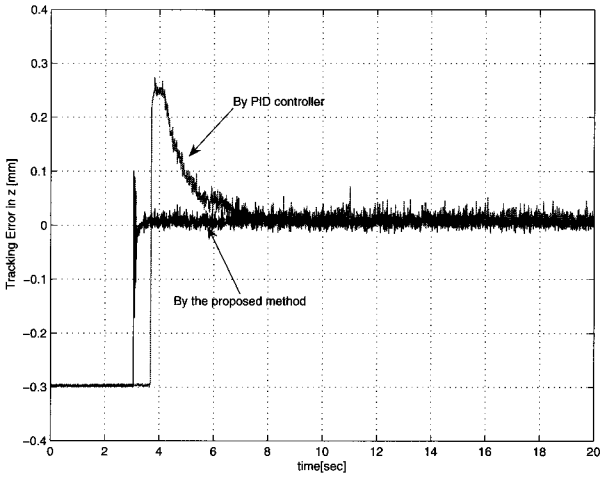

그림 8. 양 방법에 의한 제어 오차의 비교.

Fig. 8. Tracking error comparison of both methods.

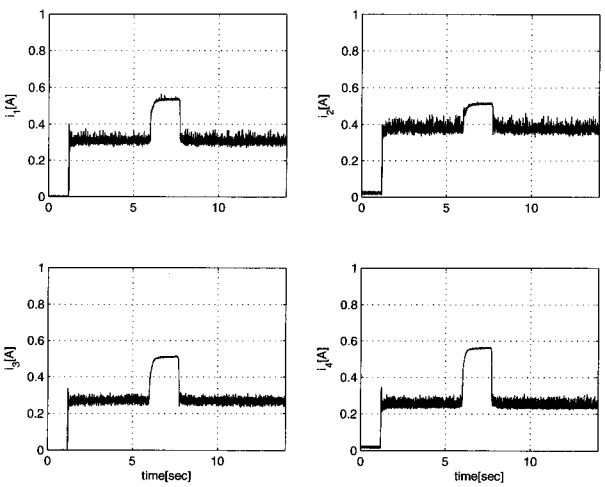

그림 9. 제안된 방법으로의 결과 - 외란에 대한 로터의 반응.

Fig. 9. Control result by the proposed method - behavior of the rotor under the external disturbance.

gain-scaling factor is proposed and high-gain observer is used in order to estimate the velocity of z, ϕ, θ. Experiment results show that the proposed controller achieves the accurate positioning of the rotor under the narrow gap condition, which is a suitable result for magnetic bearing wheels. The proposed nonlinear control approach exhibits better performance over the conventional PID control approach. Moreover, the stability analysis with a simple systematic controller design procedure is given. Also, the robustness is tested under the external disturbance. Under the current system, the FTM supports only the attractive forces for the rotor, thus the repulsive force cannot be generated. Moreover, it is necessary to have x, y-transitional motion and z-rotational motion for the rotor to be an actual candidate for magnetic reaction wheels. As a future research topic, the hardware set for generating repulsive force, x, y-transitional motion, z-rotational motion will be developed in the next development stage.

VI. APPENDIX

Consider the following SISO system

$$\begin{aligned} \dot{x} &= Ax + Bu + \delta(t,x,u) \\ y &= Cx \end{aligned} \tag{22}$$

where $x \in R^n$ is state, (u, y) is an input and output pair, (A, B) is a Brunovsky canonical pair, $C = [1,0,\cdots,0]$, and $\delta(t,x,u) = [\delta_1(t,x,u),\cdots,\delta_n(t,x,u)]^T$ represents system uncertainty which includes model/parameter uncertainty and disturbance, etc. Note that the system (22) represents a class of feedback linearized system with uncertainty. Suppose that this system uncertainty satisfies the following triangularity condition:

$$\delta_i(t,x,u) \le c(|x_1| + \cdots + |x_i|), \quad i = 1,\cdots,n \tag{23}$$

Then, the following controller with a gain-scaling factor ε_K stabilizes the system (22) when $A + B[k_1,\cdots,k_n]$ is Hurwitz (see (12)) and ε_K is sufficiently small $(\varepsilon_K << 1)$ [11]:

$$u = K(\varepsilon_K)x,\ K(\varepsilon_K) = \left[\frac{k_1}{\varepsilon_K^n},\cdots,\frac{k_n}{\varepsilon_K}\right],\ \varepsilon_K > 0 \tag{24}$$

In particular, by following the stability analysis in [11], with $V(x) = x^T P(\varepsilon_K)x$ with $A_K^T P + PA_K = -I$, $P(\varepsilon_K) = E(\varepsilon_K)$ $PE(\varepsilon_K)$, $E(\varepsilon_K) = \mathrm{diag}[1,\varepsilon_K,\cdots,\varepsilon_K^{n-1}]$ where A_K is Hurwitz, we can obtain that

$$\dot{V}(x) \le -(\varepsilon_K^{-1} - c(1 + \cdots + \varepsilon_K^{n-1}))\,\|E(\varepsilon_K)x\|^2 \tag{25}$$

Thus, ε_K is chosen to suppress the uncertainty and also tuned for faster system response.

Then, the controller (24) is combined with a high-gain observer [12,14] to make the overall controller robust and have fast system response. Thus, the effect cause by system uncertainty becomes negligible by suppressing it. The robustness analysis of observer is very similar to the analysis for controller. In summary, similarly to controller case, when $A + [l_1,\cdots,l_n]^T C$ is Hurwitz (see (10) and ε_L is sufficiently small $(\varepsilon_L << 1)$, the observer robustly converges to actual state values. The more detailed theoretical backgrounds regarding the effect of gain-scaling factors ε_K, ε_L are addressed in [11,12] (see Corollary 1).

REFERENCES

[1] Y. Park, M.-J. Tahk, M.-R. Nam, I.-H. Seo, S.-H. Lee, and J.-T. Lim, "Least squares based PID control of an electromagnetic suspension system," *KSAS Int.* Journal, vol. 4, no. 2, pp. 69-78, 2003.

[2] O.-S. Kim, S.-H. Lee, and D.-C. Han, "Positioning performance and straightness error compensation of the magnetic levitation stage supported by the linear magnetic bearing," *IEEE Trans. Ind. Electron.*, vol. 50, no. 2, pp. 374-378, 2003.

[3] L. Li, T. Shinshi, and A. Shimokohbe, "Asymptotically exact linearizations for active magnetic bearing actuators in voltage control configuration," *IEEE Trans. Contr. Syst. Technol.*, vol. 11, no. 2, pp. 185-195, 2003.

[4] J.D. Lindlau and C.R. Knospe, "Feedback linearization of an active magnetic bearing with voltage control," *IEEE Trans. Contr. Syst. Technol.*, vol. 10 no. 1, pp. 21-31, 2002.

[5] A.E. Hajjaji and M. Ouladsine, "Modeling and nonlinear control of magnetic levitation systems," *IEEE Trans. Ind. Electron.*, vol. 48, no. 4, pp. 831-838, 2001.

[6] S.J. Joo and J.H. Seo, "Design and analysis of the nonlinear feedback linearizing control for an electromagnetic suspension system," *IEEE Trans. Contr. Syst. Technol.*, vol. 5, no. 1, pp. 135-144, 1997.

[7] S.-H. Lee, H.-K. Sung, J.-T. Lim,, and Z. Bien, "Self-tuning control of electromagnetic levitation systems," *Contr. Engr. Practice*, vol. 8, pp. 749-756, 2000.

[8] P.K. Sinha, *Electromagnetic Suspension: Dynamics and Control*, Peter Peregriunus Ltd., London, 1987.

[9] D.L. Trumper, S.M. Olson, and P.K. Subrahmanyan, "Linearizing control of magnetic suspension systems," *IEEE Trans. Contr. Syst. Technol.*, vol. 5, no. 4, pp. 427-438, 1997.

[10] Z.-J. Yang and M. Tateishi, "Adaptive robust nonlinear control of a magnetic levitation system," *Automatica*, vol. 37, pp. 1125-1131, 2001.

[11] H.-L. Choi and J.-T. Lim, "On robust approximate feedback linearization," *IEICE Trans. Fundamentals*, vol. E87-A, no. 2, pp. 502-504, 2004.

[12] H.-L. Choi and J.-T. Lim, "Global exponential stabilization of a class of nonlinear systems by output feedback," *IEEE Trans. Automat. Contr.*, vol. 50, no. 2, pp. 255-257, 2005.

[13] A.M. Dabroom and H.K. Khalil, "Output feedback sampled-data control of nonlinear systems using high-gain observers," *IEEE Trans. Automat. Contr.*, vol. 46, no. 11, pp. 1712-1725, 2001.

[14] H.K. Khalil, *Nonlinear Systems*, 3rd Ed. Prentice-Hall, Inc., Upper Saddle River, NJ 07458, 2002.

[15] S. Xepapas, A. Kaletsanos, F. Xepapas, and S. Manias, "Sliding-mode observer for speed-sensorless induction motor drives," *IEE Proc.-Control Theory Appl.*, vol. 150, no. 6, pp. 611-617, 2003.

최 호 림

1996년, Univ. of Iowa, USA(학사). 1999년, 2004년 KAIST(석/박사). KAIST 정보전자연구소 박사 후 연구원, 연구조교수. KIST 인지로봇연구단 선임연구원. 2007년~현재 동아대학교 전기공학과 조교수. 관심분야는 비선형 시스템의 궤환 선형화기법, 시지연 시스템, DEDS 등.

구 민 성

2004년, 2006년 KAIST(학/석사). 현재 KAIST 박사과정 재학중. 관심분야는 비선형 시스템의 궤환 선형화 기법, switching 기법.

김 용 민

2004년, 2006년 KAIST(학/석사). 현재 KAIST 박사과정 재학중. 관심분야는 Space Robotics, Manipulator Control.

신 희 섭

2002년, 2004년, 2009년 KAIST(학/석/박사). 현재 LIG 넥스원 선임연구원. 관심분야는 SAR 신호처리, 요동보상기법.

임 종 태

제어 · 자동화 · 시스템공학 논문지 제6권 제8호 참조.